New Insights of Historical Mortars Beyond Pompei: The Example of *Villa del Pezzolo*, Sorrento Peninsula

Concetta Rispoli [1,*], **Sossio Fabio Graziano** [2], **Claudia Di Benedetto** [1], **Alberto De Bonis** [1], **Vincenza Guarino** [1], **Renata Esposito** [3], **Vincenzo Morra** [1] **and Piergiulio Cappelletti** [1]

[1] Dipartimento di Scienze della Terra, dell'Ambiente e delle Risorse, Università di Napoli Federico II-Complesso Universitario Monte Sant'Angelo, Ed. L, Via Cintia 26, 80126 Napoli, Italy; claudia.dibenedetto@unina.it (C.D.B.); alberto.debonis@unina.it (A.D.B.); vincenza.guarino@unina.it (V.G.); vincenzo.morra@unina.it (V.M.); piergiulio.cappelletti@unina.it (P.C.)

[2] Dipartimento di Farmacia, Università degli Studi di Napoli Federico II-Via D. Montesano 49, 80131 Napoli, Italy; sgraziano@unina.it

[3] Dipartimento di Studi Umanistici, Università degli Studi di Napoli Federico II-Via Porta di Massa 1, 80133 Napoli, Italy; renataesp@libero.it

* Correspondence: concetta.rispoli@unina.it; Tel: +39-0812538176

check for updates

Abstract: The topic of this study is the archaeometric characterization of mortars from *Villa del Pezzolo*, a Roman Villa located in Seiano (Napoli-Campania, Italy), dated between the 1st century B.C. and the 3rd century A.D. Mortars were analyzed by means of a multi-analytical approach (polarized optical microscopy, X-ray powder diffraction, scanning electron microscopy and energy-dispersed spectrometry, thermal analyses and mercury intrusion porosimetry) according to existing recommendations. Analytical results evidenced the use of local geomaterials composed of sedimentary and volcanic aggregates in the mix design and confirmed the three distinct building phases identified by archaeologists. Volcanic tuff fragments, identified in the 1st building phase can be ascribed to Campanian Ignimbrite formation, widely cropping out in the Sorrento Peninsula, as confirmed by the presence of glassy shards, partially devitrified and replaced by authigenic feldspar, a typical feature of welded grey ignimbrite lithofacies (WGI). Volcanic aggregates in samples of the 2nd and 3rd building phases show, instead, the presence of leucite-bearing volcanic scoriae and garnet crystal fragments related to Somma-Vesuvius products. Study of these mortars allowed us to: (1) understand the production technologies; (2) highlight use of materials with hydraulic behavior, such as volcanic and fictile fragments; (3) confirm the three building phases from compositional features of mortars and (4) highlight the change over time of the volcanic aggregate for mortars mix-design.

Keywords: ancient mortars; archaeometry; multi-analytical characterization; sorrento peninsula; *Villa del Pezzolo*; hydraulicity index; constructive phases; production technology; raw materials

1. Introduction

The Bay of Naples (Figure 1a) is characterized by the presence of several worldwide known archaeological sites [1–4] and references therein, some of them are very interesting and well preserved, among which Pompeii represents, by far, an almost unique example of a still-visible ancient town. Nevertheless, minor, but not for importance, sites (villas, cisterns, *thermae,* necropolis, etc.) are widespread all over the area.

Villa del Pezzolo is a Roman villa, located in Seiano, which represents a good example of a Patrician villa (Figure 1a,b). The villa was inhabited throughout four centuries, between the 1st century B.C. to 3rd century A.D. During that period, there were more reconstruction phases following catastrophic

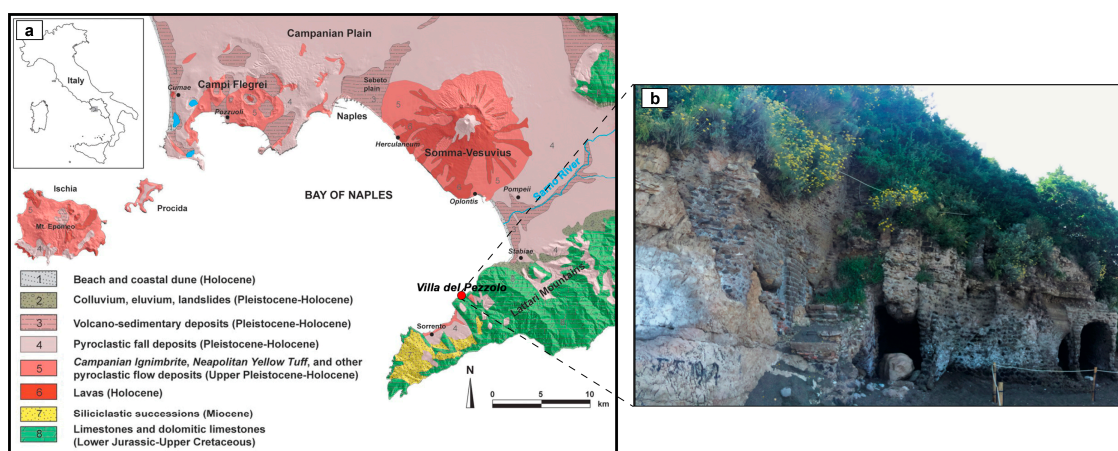events such as the 62 A.D. earthquake, the 79 A.D. eruption of the Somma-Vesuvius and subsequent debris flow.

Figure 1. (**a**) Geological sketch map of Bay of Naples area (modified after [1]) with the location of the archaeological site *Villa del Pezzolo*; (**b**) picture of *Villa del Pezzolo*.

The site is very interesting both for archaeologists and geologists, as it also represents one of the few locations along Sorrento Peninsula coastline where the consequences of A.D. 79 Somma-Vesuvius eruption are clearly visible, despite the distance from the eruptive center [5].

Like other remarkable examples existing in the Bay of Naples, this villa has been preserved until now, even though located in an aggressive environment by the seaside, thanks to the construction expertise of Roman workers. In particular, thanks to the use of hydraulic mortars. Ancient mortars are composite materials with both crystalline and amorphous phases, containing inerts and reactive aggregates in a calcitic binder [6], which were in use until the end of the 19th century, when Portland cement first appeared [7]. The greatest interest on these artificial geomaterials is certainly due to ancient Roman builders and, mainly, to their skills in using well-defined materials such as *pozzolana* and fictile fragments in the mix design [8].

The main source of information about the Roman technical ability for manufacturing these materials is the treatise "*De Architectura*" by *Marcus Vitruvius Pollio* (80–15 B.C.), dedicated to emperor *Augustus*. This treatise, namely the second book, describes in detail the utilized materials in the construction sector, including those necessary for mortars production.

The excellent conservation state of many products made in the Roman period demonstrates the high technological level achieved by these builders. Roman builders knew that, thanks to the combination of the lime with special volcanic deposits (*pozzolana*), mortar became hydraulic, and it means allowing underwater hardening and also acquiring a greater mechanical strength [8–10]. Another very important skill was the possibility to use, whenever volcanic materials were not available, fragments of artificial fictile fragments, such as bricks, pottery or shattered tiles, which have the same hydraulic properties of *pozzolana* [8].

Studies on Roman mortars are very interesting to understand the "secrets" of such enduring resistance because, as of today, the Villae or other Roman buildings have resisted over two thousand years the impact of waves and weathering due to seawater [11–15]. Thus, Roman mortars represent a tangible example of a long-lasting transformation product of geological raw materials.

Nowadays, the concept of "durability" is still of great interest. The modern concrete technologists try to constantly improve their formulation to replicate Roman concrete features such as strength and resistance against aggressive agents (i.e., seawater chemical and mechanical action, acid rains, etc.; [16]).

This research aims to: (a) characterize the mortars used in the construction of *Villa del Pezzolo* in order to improve knowledge about Roman construction material manufacturing by means of a detailed

microstructural and compositional examination of the cementiceous binding matrix and aggregates, (b) identify the mix design and provenance of raw materials; and (c) highlight the minerogenetic secondary processes.

2. Geological and Archaeological Background

Villa del Pezzolo is placed in a pocket beach along the north shore of the Sorrento Peninsula in a tiny bay called Marina di Equa (Seiano), in the northern flank of Lattari Mounts, constituting the southern margin of the Campanian plain (Figure 2a), [5,17].

The geological evidence of the Campanian plain are mostly related to tectonic extensional movements and volcanoclastic events [18]. The Lattari Mounts are placed 20 km south of the Somma-Vesuvius volcano and 40 km south of Naples (Italy). This mountain ridge is composed by Mesozoic limestones covered by late Quaternary ashfall deposits belonging to the A.D. 79 eruption of Somma-Vesuvius (Figure 2a), [19].
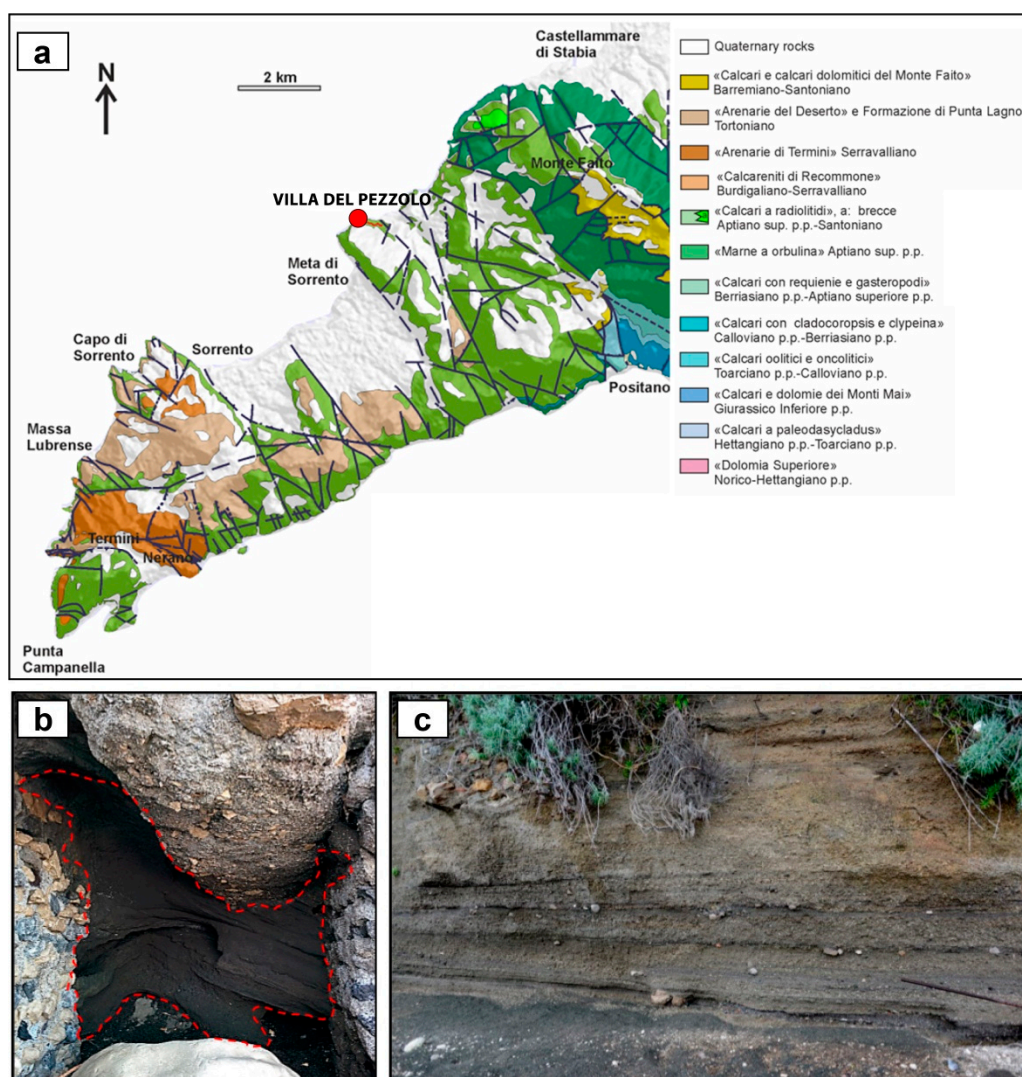
Figure 2. (**a**) Geological sketch map of Sorrento Peninsula (modified after [17]); (**b**) evidence of A.D. 79 eruption: base surge of Somma-Vesuvius volcano (~12 km far); (**c**) "Durece" deposit, typical lithofacies of reworked pyroclastic deposits.

On the archaeological site, the impact of the A.D. 79 Somma-Vesuvius eruption is clearly visible. This geographical area was affected by of two phases with relative different deposits: primary,

the sedimentary records related to base surge events which caused the formation of pyroclastic deposits (Figure 2b), [18]; secondary, the alluvial delta, called "Durece deposition" [19] by the local population, caused by alluvial events, following the volcanic eruption. This event caused the erosion of volcanic deposits [20] and the consequent burial of the villa. Later, the alluvial delta was broken down creating a 6–8 m high "Durece" cliff, still present on the beach (Figure 2c) [19].

Moreover, the marine erosion processes seriously damaged the building, making it is impossible to recognize the original construction plan. However, analysis of geological stratigraphy [5] and masonry techniques confirms the archaeological hypothesis of three building phases (Figure 3), [21].

The first building phase was dated back from the 1st century B.C. to the 79 A.D. (Somma-Vesuvius eruptive event; Figure 3b) and is identifiable by the presence of masonry works in *opus vittatum* and *opus reticulatum*. The first *opus* became widespread during the Augustan age while the second one was used in southern Italy between the 1st century B.C. and the 1st century A.D. [18,22].

The villa was built on a limestone flank with a staircase, descending to the seaside, deeply damaged and buried by the eruptive products at the end of the first phase.

In the second phase, dated to the first half of 2nd century A.D. (Figure 3c), after a series of flood events, the villa was completely buried and rebuilt and some rooms were restored using the *opus reticulatum* with small elements [18–22]. This led to the creation of new spaces, different in form and orientation with respect to the original core structure (Figure 3c) [18–23]. This information is supported by the evidence that the walls of the second phase are not in line with the remnants of the first phase structures (Figure 3a) [5].
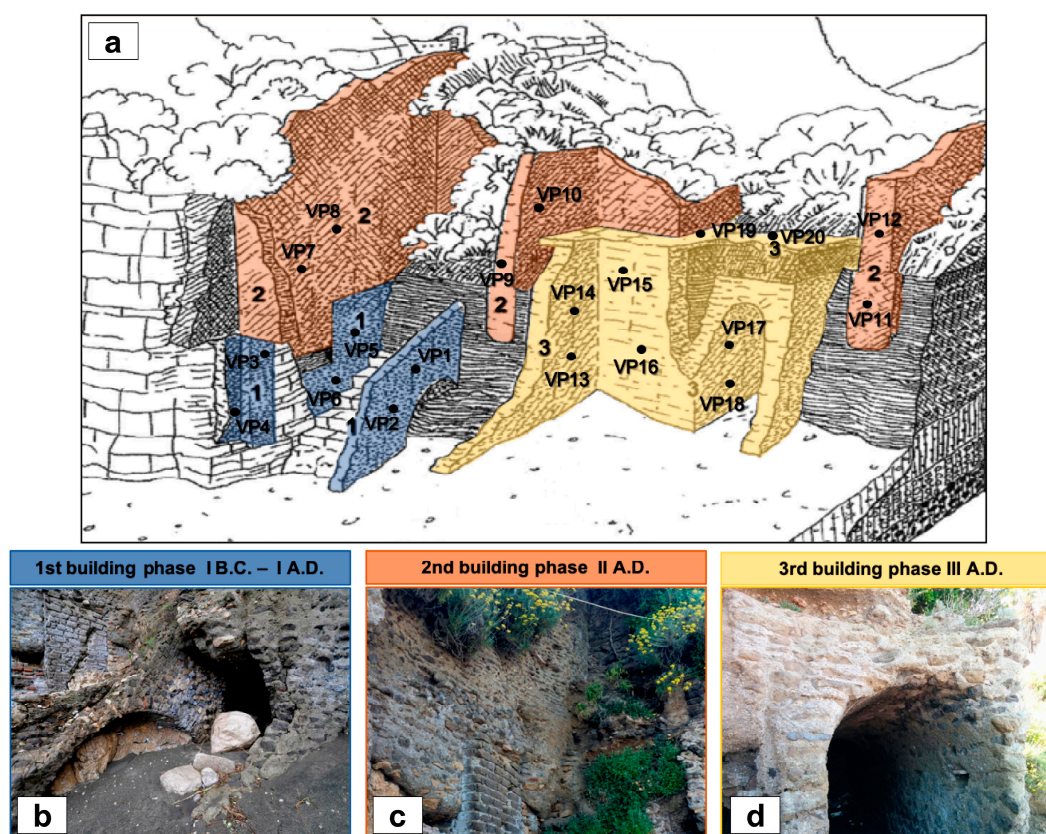
Figure 3. (**a**) Sketch of the *Villa del Pezzolo* archaeological remains on the beach (modified after [18]) with sampling points; (**b**) 1st building phase; (**c**) 2nd building phase; (**d**) 3rd building phase.

After this phase, new spaces were damaged and, in some cases, destroyed by sea action, probably due to their position on an alluvial delta [18]. Finally, a third phase (3rd century A.D.; Figure 3d) consisted in the building of a new access to the sea and in restoration of rooms resting on the terrace [18].

The decoration of the roman villa is documented by some sporadic marble findings, now kept at the National Archaeological Museum of Naples.

3. Materials and Methods

Sampling (20 mortars) was performed on several walls of the archaeological complex (Figure 3), i.e., thanks and with the assistance of archaeologists of the former *Soprintendenza per i Beni Archeologici della Campania* in order to take samples that were representative of the construction. The sampling was carried out by hammer and criteria such as the type of mortar, the good state of aggregation, the available quantities and little invasivity.

The collected samples consist of eighteen bedding mortars and two floor mortars (Figure 3a), and were grouped following the building phases (group A—1st building phase, group B—2nd building phase and group C—3rd building phase; Figure 3a; Table 1).

Table 1. List of the mortar samples with relative typology, group, building phase, and probable dating defined by literature information.

Samples	Typology	Group	Building Phase	Probable Dating
VP1	bedding mortar	A	1st	I century B.C.-I century A.D.
VP2	bedding mortar	A	1st	I century B.C.-I century A.D.
VP3	bedding mortar	A	1st	I century B.C.-I century A.D.
VP4	bedding mortar	A	1st	I century B.C.-I century A.D.
VP5	bedding mortar	A	1st	I century B.C.-I century A.D.
VP6	bedding mortar	A	1st	I century B.C.-I century A.D.
VP7	bedding mortar	B	2nd	II century A.D.
VP8	bedding mortar	B	2nd	II century A.D.
VP9	bedding mortar	B	2nd	II century A.D.
VP10	bedding mortar	B	2nd	II century A.D.
VP11	bedding mortar	B	2nd	II century A.D.
VP12	bedding mortar	B	2nd	II century A.D.
VP13	bedding mortar	C	3rd	III century A.D.
VP14	bedding mortar	C	3rd	III century A.D.
VP15	bedding mortar	C	3rd	III century A.D.
VP16	bedding mortar	C	3rd	III century A.D.
VP17	bedding mortar	C	3rd	III century A.D.
VP18	bedding mortar	C	3rd	III century A.D.
VP19	floor mortar	C	3rd	III century A.D.
VP20	floor mortar	C	3rd	III century A.D.

The collected samples were characterized according to [24] European standard.

Macroscopic characteristics, such as color, presence of aggregates, and others, were observed in order to identify materials and to plan the analytical approach, performed at DiSTAR (*Dipartimento di Scienze della Terra, dell'Ambiente e delle Risorse, Università di Napoli Federico II*) laboratories and at the Group Technical Center (CTG) of the company Italcementi Heidelberg Group in Bergamo (Italy). Color was evaluated by comparison with the Munsell Soil Color Chart [25].

Polarized optical microscopy (POM) on thin sections was performed using a Leica DFC280 microscope (Leica, Wetzlar, Germany) to observe the textural features and the petrographic composition of samples. The percentage of binder and aggregate was measured by modal analysis, counting at least 1500 points for each section, using Leica Q Win image analysis software (version 3.2.1, Leica, Wetzlar, Germany). This analysis can be considered representative since the maximum uncertainty of percentage for a total amount of 1500 points is about 2.8% [26].

Mineralogical determinations were performed on different fractions: binder, aggregates and fictile fragments, according to [24]. Mortars were gently disaggregated and separated in different fractions using a binocular microscope (WILD M38, Heerbrugg, Switzerland). Each fraction was

powdered in an agate mortar to obtain a homogeneous sample to acquire (particle size< 200 μm) avoiding orientation related problems, primary extinction or crystallite size errors [27,28]. Qualitative mineralogical analyses were performed by X-ray powder diffraction (XRPD) using a PANalytical X'Pert PRO 3040/60 PW diffractometer (Malvern PANalytical, Almelo, The Netherlands) CuKα radiation, 40 kV, 40 mA, scanning interval 4–70° 2θ, equivalent step size 0.017° 2θ, with a step counting time of 120 s. To identify the mineral phases, the PANalytical Highscore Plus 3.0e software (Malvern PANalytical, Almelo, The Netherlands) with PDF-2/ICSD databases was used.

Micro-textural observations and quantitative micro-chemical analyses were carried out by Scanning Electron Microscopy coupled with Energy Dispersive Spectroscopy (SEM/EDS; JEOL JSM-5310 (Jeol Ltd., Tokyo, Japan) coupled with a Oxford Instruments Microanalysis Unit (Oxford Instruments plc, Abingdon, Oxfordshire, UK) equipped with an INCA X-act detector (ETAS group, Stuttgart, Germany). Measurements were performed with an INCA X-stream pulse processor (ETAS group, Stuttgart, Germany) using a 15 kV primary beam voltage, 50–100 μA filament current, variable spot size, from 30,000 to 200,000× magnification, 20 mm WD and 50 s net acquisition real time. The INCA Energy software (ETAS group, Stuttgart, Germany) was employed, using the XPP matrix correction scheme and the Pulse Pile up correction. The quant optimization was carried out using cobalt (FWHM—full width at half maximum peak height- of the strobed zero = 60–65 eV). The following standards from the Smithsonian Institute and MAC (Micro-Analysis Consultants Ltd. St Ives, UK) were used for calibration: diopside (Ca), fayalite (Fe), San Carlos olivine (Mg), anorthoclase (Na, Al, Si), rutile (Ti), serandite (Mn), microcline (K), apatite (P), fluorite (F), pyrite (S), sodium chloride (Cl), benitoite (Ba) and pure vanadium (V), [29]. The Kα, Lα, Lβ, or Mα lines were used for calibration, depending on the specific element.

High-resolution imaging of surface morphology (backscattered images) was generated by secondary electrons using the same instrument.

Micro-chemical analyses (EDS) were performed to determine chemical composition of binder and lime lumps and to study volcanic fragments identified among aggregates (point data). The Hydraulicity Index (HI) of binder and lime lumps was calculated according to Boynton [30] using (SiO_2 + Al_2O_3 + Fe_2O_3)/(CaO + MgO) ratio.

The thermal behavior of mortars was carried out with a Mettler Toledo TGA/SDTA 851e instrument (Mettler Toledo, Columbus, OH, USA). The samples were heated from 40 °C to 1000 °C, with a heating rate of 10 °C/min in nitrogen atmosphere (flow rate 60 mL/min), with the main goal of determining the total (binder plus aggregates) hydraulic features of these materials. TG and DSC curves were acquired and then processed with Mettler Toledo STARe SW 7.01 software (Mettler Toledo, Columbus, OH, USA). Thermal analyses were performed on powered bulk samples and on their finer sieved fraction (<63 μm); the latter can be considered as a binder-enriched specimen [31].

The pore system of samples was investigated by means of Mercury Intrusion Porosimetry (MIP). Due to the scarce amount and small dimensions of samples, four samples, approximately 1 cm^3 in size, were selected on the bases of macroscopic and microscopic features. Analyses were performed on three fragments for each sample, and average results are reported. These fragments were dried in an oven for 24 h at 105 °C and then analyzed by Thermo Scientific equipment PASCAL 140 (Thermo Fisher Scientific, Waltham, MA, USA) with a maximum injection pressure of 0.4 MPa and PASCAL 240 with a maximum injection pressure of 200 MPa. These instruments, used consecutively, allowed us to assess (1) total volume of pores with a radius between 3.75 nm and 800 μm (mm^3/g), (2) open porosity (vol.%), (3) bulk density (g/cm^3), (4) apparent density (g/cm^3), and (5) specific surface (m^2/g); graphical and numerical representation of the distribution of pore size was also provided.

4. Results

4.1. Texture and Optical Microscopy of the Mortar

Mortar samples appear to be macroscopically intact and quite hard (Figure 4).

Bedding mortars made evident yellow to dark greyish brown colors (Munsell 2.5Y 7/3 to 10YR 4/2), with coarse aggregates ranging from 2 mm up to 3 cm (Figure 4a). The aggregates were made of volcanic and carbonate fragments and, only in samples of the group C, fictile fragments were recognized (Figure 4b). Floor mortars showed a variability in color from very pale brown to reddish (Munsell 7.5YR-7/3 to 5YR-5/6). The aggregates mainly comprised of fictile fragments and subordinately by volcanic and carbonate fragments, variable in size from 1 mm to 2.5 cm. All mortars contained lime lumps (2–4 mm) that generally consisted of unreacted lime [31].
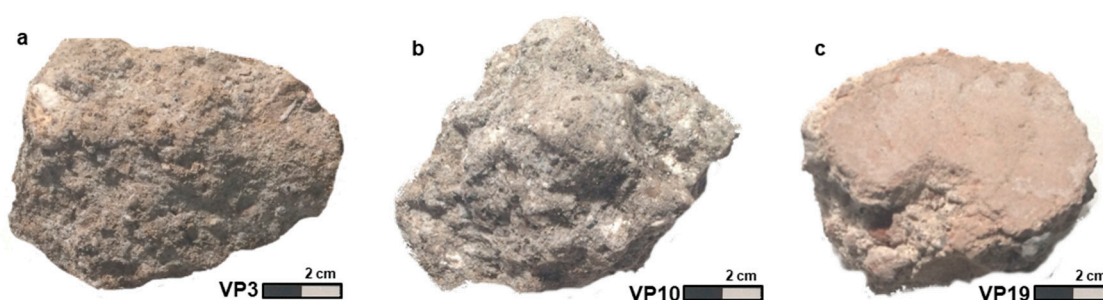

Figure 4. Some representative mortar samples from archaeological sites; (**a**) VP3 bedding mortar sample (group A); (**b**) VP10 bedding mortar sample (group B); (**c**) VP19 floor mortar sample (group C).

Thin section observations showed that the mortars of group A were characterized by cryptocrystalline and micritic binder, respectively (35.4 vol.%; 12.6 vol.%; Figure 5a). Small and fractured lime lumps were also observed (3.0 vol.%; Figure 5b). The aggregates were constituted mainly by pumice (13.3 vol.%), volcanic and carbonate fragments (10.6 vol.%; 2.1 vol.%), scoriae (3.7 vol.%), and crystal fragments of plagioclase, clinopyroxene and sanidine (6.5 vol.%). The shapes of aggregates were sub-angular, and their size distribution was moderately sorted.

Volcanic fragments were characterized by glassy shards partially devitrified (Figure 5c).

Group B includes mortars mainly characterized by cryptocrystalline matrix (43.8 vol.%) and a low percentage of micritic matrix (4.9 vol.%; Figure 5d).

Aggregate fraction was characterized by altered pumice (with garnet and leucite crystal fragments; 12.1 vol.%; Figure 5e), scoriae (1.2 vol.%), leucite-bearing scoriae (13.3 vol.%), volcanic fragmemts (0.9 vol.%), carbonate fragments (5.3 vol.%; Figure 5f), and crystal fragments of plagioclase, clinopyroxene (Figure 5d), sanidine, garnet and leucite (8.6 vol.%). The shape of aggregates ranged from sub-angular to sub-rounded and their size distribution was moderately sorted.

Binder phase of samples from group C was composed of cryptocrystalline matrix (28.3 vol.%) and micritic matrix (10.6 vol.%; Figure 5g) and some lime lumps (1.8 vol.%).

Aggregate fraction appeared moderately sorted and sub-rounded, composed of fictile fragments (15.5 vol.%; Figure 5g), pumice (15.0 vol.%; Figure 5h), leucite-bearing scoriae (4.6 vol.%; Figure 5h), volcanic and carbonate fragments (0.5 vol.%; 6.9 vol.%, Figure 5i), amphibole, garnet and leucite as crystal fragments (7.1 vol.%).

The floor mortars VP19 and VP20 samples, belonging to group C, were identified as *cocciopesto*, also called *opus signinum*, a typical building technique used in the ancient Rome for making floor and waterproofing cisterns. The binder phase was composed mainly of micritic matrix (25.4 vol.%) and lime lumps were also present (2.2 vol.%; Figure 5l).

Fictile fragments are different from each other, even if included in a single mortar sample. In particular, fictile matrices can be either characterized by high (Figure 5g) or low (Figure 5l) optical activity. In some fictile fragments, inclusions are mainly represented by tiny crystals of quartz, biotite, clinopyroxene (Figure 5m), whereas, in other fragments, they are characterized by a prevailing volcanic component (pumice and scoriae; Figure 5n).

Modal analysis (Table 2) highlighted the differences in the aggregate/binder ratio, particularly evident in group C. Mortars of this group showed a binder/aggregate ratio lower than 1, indicating a higher percentage of aggregates than the binder phase.

Table 2. Petrographic features of the samples and their microscopic modal analysis—mineral abbreviations from Whitney and Evans [32].

Mortars	(Group A)	(Group B)	(Group C)	(Group C-Floor Mortar)
Constituents (vol.%)				
Feldspars (Sa, Pl)	3.4	2.6	2.3	3.1
Mafic Minerals (Cpx, Amp, Bt)	3.1	6.0	4.8	5.9
Garnets	-	0.3	1.6	1.2
Volcanic fragments	10.6	0.9	0.5	0.8
Scoriae	3.7	1.2	1.3	0.7
Leucite-bearing scoriae	-	13.3	4.6	3.7
Pumice	13.3	12.1	15.0	17.3
Fictile fragments	-	-	15.5	16.2
Carbonate fragments	2.1	5.3	6.9	4.5
Lime lumps	3.0	1.8	1.8	2.2
Micritic matrix	12.6	4.9	10.6	25.4
Cryptocrystalline matrix	35.4	43.8	28.3	11.3
Macroporosity	12.1	7.3	6.4	7.0
Others	0.6	0.6	0.6	0.7
Total points%	100.0	100.0	100.0	100.0
Total Binder%	51.0	50.6	40.6	38.9
Total Aggregate%	36.3	41.6	52.4	53.4
Binder/Aggregate ratio	1.4	1.2	0.8	0.7

Abbreviations: Sa: sanidine; Pl: plagioclase; Cpx: clinopyroxene; Amp: amphibole; Bt: biotite.
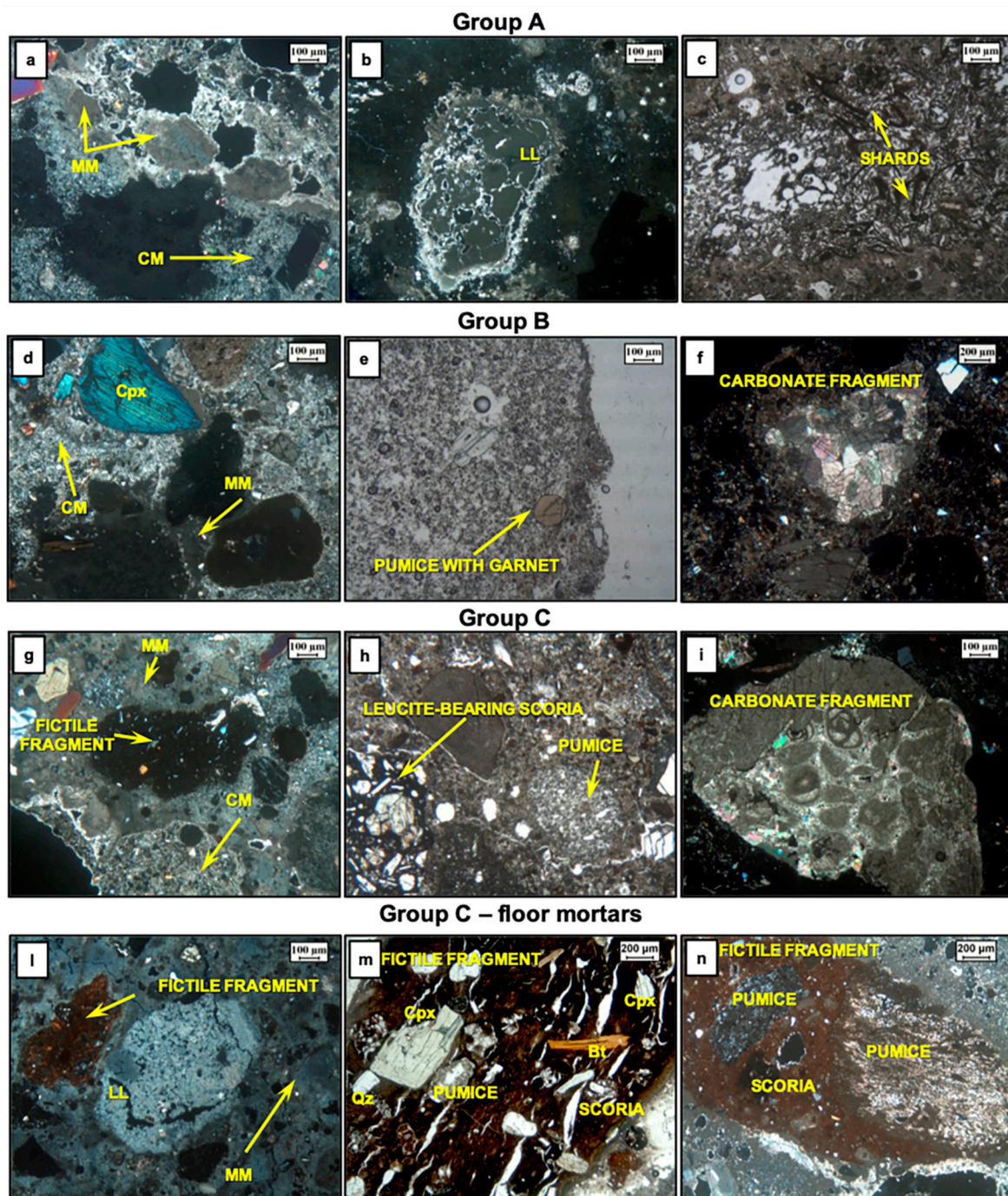
Figure 5. Microphotographs of mortar components (in CPL: Cross Polarized Light; PPL: Plane Polarized Light). Abbreviations: MM: micritic matrix; CM: Cryptocrystalline matrix; LL: lime lump; Cpx; clinopyroxene; Bt: biotite; Qz: quartz. Group A: (**a**) micritic matrix and cryptocrystalline matrix (CPL) in VP3 sample; (**b**) lime lump (CPL) in VP2 sample; (**c**) glassy shards in volcanic aggregates (PPL) in VP3 sample; group B: (**d**) micritic matrix, cryptocrystalline matrix and clinopyroxene (CPL) in VP8 sample; (**e**) pumice with garnet (PPL) in VP12 sample; (**f**) marble fragment (CPL) in VP7 sample; group C: (**g**) cryptocrystalline matrix, micritic matrix and fictile fragment (CPL) in VP15 sample; (**h**) leucite-bearing scoria and pumice (PPL) in VP17 sample; (**i**) carbonate rich sedimentary rock fragment (CPL) in VP18 sample; group C-floor mortars; (**l**) micritic matrix, lime lump and fictile fragment (CPL) in VP19 sample; (**m,n**) different types of fictile fragments (CPL) in VP20 sample.

4.2. Mineralogical Analyses

The collected samples were separated into binder, aggregates, and fictile fragments, according to [24] recommendation (mortar characterization) and then analyszd by XRPD. Results are shown in Table 3 and in Figure 6.

Table 3. Qualitative mineralogical composition of samples, XRPD analysis—mineral abbreviations from Whitney and Evans [32].

Samples	Group	Main Binder Phases	Main Aggregate Phases	Main FictileFragments Phases	Other Phases
VP1	group A	Cal	Anl, Sa, Pl, Cpx, Mca, Cal		Hl
VP2	group A	Cal, Gp	Cbz, Anl, Sa, Pl, Cpx, Mca, Cal		Hl
VP3	group A	Cal, Gp	Anl, Sa, Pl, Cpx, Mca, Cal		Hl
VP4	group A	Cal, Gp	Cbz, Sa, Pl, Cpx, Mca, Cal		Hl
VP5	group A	Cal, Gp	Anl, Sa, Pl, Cpx, Mca, Cal		Hl
VP6	group A	Cal, Gp	Cbz, Anl, Sa, Pl, Cpx, Mca, Cal		Hl
VP7	group B	Cal	Anl, Lct, Sa, Pl, Cpx, Mca, Cal		Hl
VP8	group B	Cal	Anl, Lct, Sa, Pl, Cpx, Mca, Cal		Hl
VP9	group B	Cal, Gp	Anl, Sa, Pl, Cpx, Mca, Cal		Hl
VP10	group B	Cal	Anl, Lct, Sa, Pl, Cpx, Mca, Cal		Hl
VP11	group B	Cal, Gp	Anl, Lct, Sa, Pl, Cpx, Mca, Cal		Hl
VP12	group B	Cal	Anl, Sa, Pl, Cpx, Mca, Cal		Hl
VP13	group C	Cal	Anl, Lct, Sa, Pl, Cpx, Mca, Cal	Qz, Cal, Hem, Sa, Cpx, Pl	Hl
VP14	group C	Cal,Gp	Anl, Lct, Sa, Pl, Cpx, Mca, Cal	Qz, Cal, Hem, Sa, Cpx, Pl	Hl
VP15	group C	Cal	Anl, Sa, Pl, Cpx, Mca, Cal	Qz, Cal, Hem, Sa, Pl	Hl
VP16	group C	Cal, Gp	Anl, Lct, Sa, Pl, Cpx, Mca, Cal	Qz, Cal, Hem, Sa, Cpx, Pl	Hl
VP17	group C	Cal	Anl, Sa, Pl, Cpx, Mca, Cal	Qz, Cal, Hem, Sa, Cpx	Hl
VP18	group C	Cal, Gp	Anl, Lct, Sa, Pl, Cpx, Mca, Cal	Qz, Cal, Hem, Sa, Cpx, Pl	Hl
VP19	Group C-Floor mortar	Cal	Anl, Sa, Pl, Cpx, Mca, Cal	Qz, Cal, Hem, Sa, Cpx, Pl	Hl
VP20	Group C-Floor mortar	Cal, Gp	Anl, Sa, Pl, Cpx, Mca, Cal	Qz,Cal, Hem, Sa, Cpx, Pl	Hl

Abbreviations: Cal: calcite; Gp: gypsum; Anl: analcime; Sa: sanidine; Pl: plagioclase; Cpx: clinopyroxene; Mca: mica; Lct: leucite; Qz: quartz; Hem: hematite; Hl: halite.
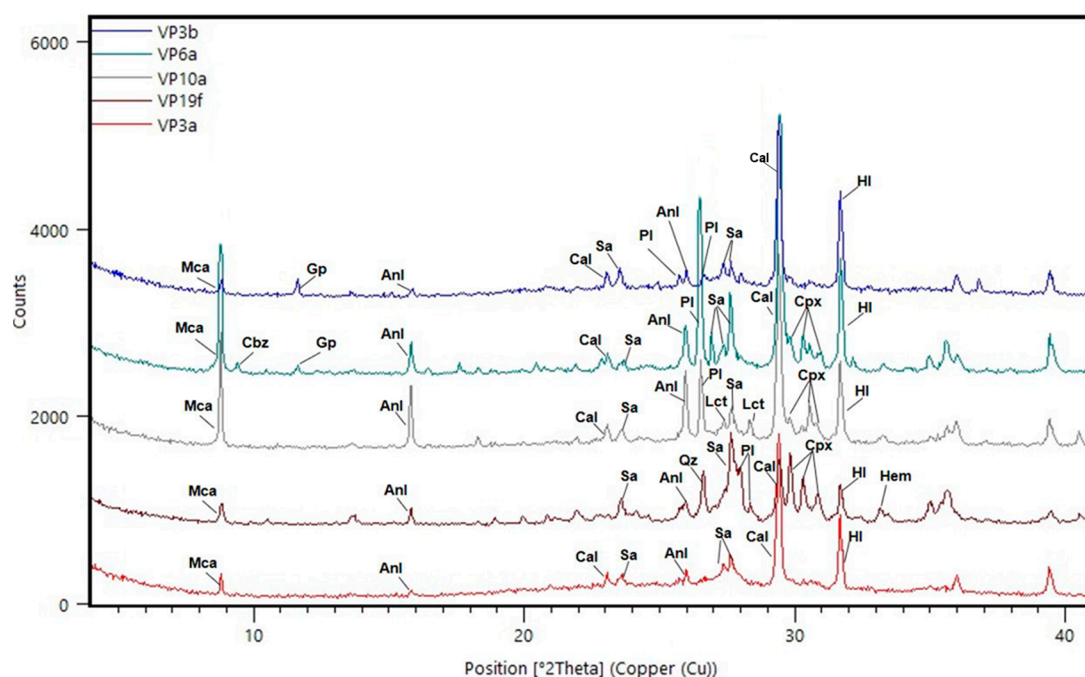

Figure 6. Qualitative mineralogical analysis of mortars. XRPD patterns of selected samples of mortars. VP3b: VP3 binder fraction (Group A); VP6a: VP6 aggregates fraction (Group A); VP10: VP10 aggregates fraction (Group B); VP19f: VP19 fictile fraction (Group C); VP3a: VP3 aggregates fraction (Group A). Mineral abbreviations: Cal: calcite; Gp: gypsum; Anl: analcime; Sa: sanidine; Pl: plagioclase; Cpx: clinopyroxene; Mca: mica; Lct: leucite; Qz: quartz; Hem: hematite; Hl: halite.

The XRPD results showed that, in binder, calcite is the main phase with subordinate amounts of gypsum. Regarding aggregates, sanidine, plagioclase, analcime, mica, clinopyroxene and calcite were recognized; chabazite is also present in some samples of group A and leucite in samples of groups B and C (Table 3; Figure 6).

Fictile fragments, only present in mortars of group C, showed the occurrence of calcite, quartz, mica, sanidine, clinopyroxene, plagioclase and hematite. All analyzed samples showed the presence of halite (Table 3; Figure 6).

XRPD analyses also allowed for revealing the presence of amorphous fraction, recognized by the rising of pattern background between 18° and 40° of a 2θ angle. This fraction is probably related to (1) volcanic glass component (pumice and scoriae) and (2) C–A–S–H phases (calcium–aluminium–silicate–hydrate).

4.3. Micro-Morphology and Chemical Analysis

SEM-EDS analyses on binder confirmed gypsum presence in some samples and demonstrated the presence of hydraulic phases such as C–A–S–H gel, with their typical spongy morphology (Figure 7a,b) [33–35].
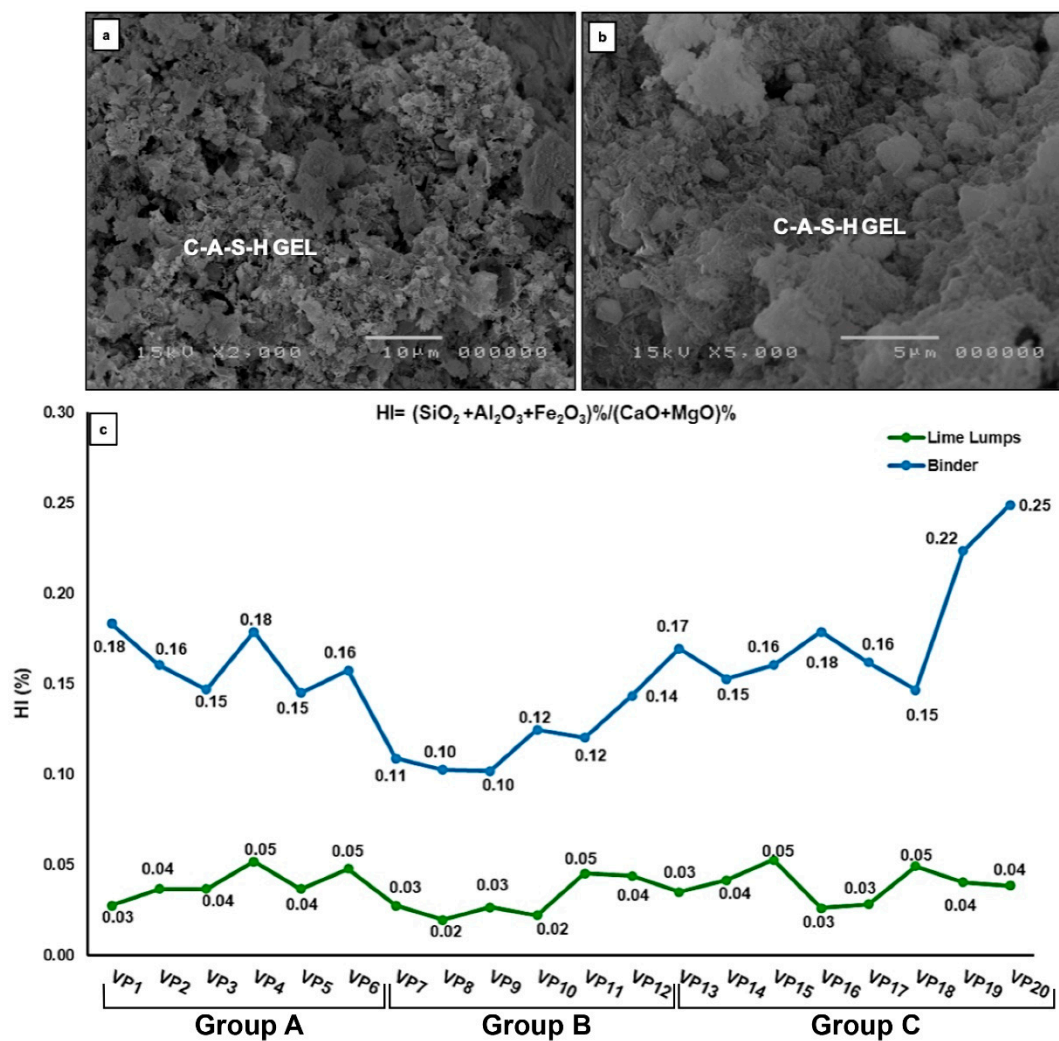

Figure 7. (**a,b**) SEM images of C–A–S–H gel in VP3 and VP6 samples; (**c**) hydraulicity Index (HI), lime lumps (green line) and binder (blue line) for analyzed mortars.

In order to obtain further information about the binder composition, SEM-EDS microanalyses were carried out on polished thin sections both on binder and on lime lumps (Tables 4 and 5). Moreover, HI was calculated, according to Boynton's formula [30], to achieve information on hydraulicity grade reached by mortars (Tables 4 and 5).

Lime lumps are composed mainly of CaO (91.15–95.10 wt.%), with very high values of CaO + MgO (92.41–97.06 wt.%; Table 4). Chemical composition of binder (Table 5) showed higher values of SiO_2 + Al_2O_3 + Fe_2O_3 (9.06–19.54 wt.%) than that of lime lumps (1.90–4.97 wt.%), as well as lower contents of CaO + MgO (78.50–89.27 wt.%).

HI of lime lumps is always lower than 0.10%, while HI of binder ranges between 0.10% and 0.25% (Figure 7c; Tables 4 and 5). VP19 and VP20 (floor mortars) samples showed, for binder, the highest HI of 0.22% and 0.25%, thus confirming their differences from all other samples.

As far as volcanic aggregates are concerned, SEM-EDS analyses highlighted for group A samples the presence of glassy shards, partially devitrified and partially coated by micrometric sanidine crystals (Figure 8a). Moreover, chemical composition of glassy shards and pumice (Supplementary Materials 1–S1) allowed us to classify them as trachyte according to the TAS diagram (Total Alkali vs. Silica) [36] (Figure 8c).

The analyses of volcanic aggregates of the second and third building phase (both dated after A.D. 79 Somma-Vesuvius eruption) showed volcanic scoriae containing abundant leucite and garnet crystal fragments (Figure 8b), both in pumice and binder. In this case, the chemical composition of pumice (Supplementary Materials 2–S2) reported in the TAS diagram (Figure 8c), allowed us to classify them as phonolite (Figure 8c).

Additional information was obtained by chemical composition of garnets that were classified as a solid solution between andradite (48.98–58.38 mol.%) and grossular (25.91–30.46 mol.%), (calculated following Locock, [37]; Supplementary Materials 3–S3).

Table 4. Major element concentrations of lime lumps (L) in *Villa del Pezzolo* mortars (in wt.%; recalculated to 100%; bdl: below detection limits). $SiO_2 + Al_2O_3 + Fe_2O_3$, $CaO + MgO$, HI (Hydraulic Index) are also shown.

wt.%	VP1 L	VP2 L	VP3 L	VP4 L	VP5 L	VP6 L	VP7 L	VP8 L	VP9 L	VP10 L	VP11 L	VP12 L	VP13 L	VP14 L	VP15 L	VP16 L	VP17 L	VP18 L	VP19 L	VP20 L
SiO_2	1.59	1.89	2.42	2.71	2.42	2.89	1.42	3.11	1.16	1.58	3.25	3.28	2.40	3.21	3.04	1.81	1.57	2.68	2.32	3.02
TiO_2	0.24	bdl	bdl	bdl	bdl	bdl	0.35	bdl	0.80	0.35	0.30	0.15	0.35	bdl	0.02	bdl	0.07	bdl	bdl	0.11
Al_2O_3	0.22	0.95	0.95	1.63	0.95	0.95	0.26	0.62	0.88	0.20	0.73	0.60	0.69	0.55	0.58	0.61	0.92	1.65	1.52	0.63
Fe_2O_3	0.80	0.65	0.07	0.52	0.07	0.65	0.16	0.18	0.52	0.37	0.31	0.29	0.26	0.20	1.35	0.07	0.17	0.23	bdl	bdl
MnO	0.22	bdl	bdl	0.12	bdl	bdl	bdl	0.23	0.16	0.31	0.24	0.16	0.21	0.23	bdl	bdl	bdl	0.06	bdl	bdl
MgO	0.68	0.26	2.15	1.28	2.15	0.26	0.87	2.98	0.70	3.30	0.70	1.20	0.84	2.24	2.14	2.15	2.05	1.26	1.87	2.35
CaO	93.83	94.65	92.16	92.60	92.16	93.65	95.32	92.07	95.10	93.34	94.01	93.93	94.79	92.87	91.85	93.81	92.46	91.15	93.50	92.70
Na_2O	0.52	0.59	0.56	0.52	0.56	0.59	0.14	0.33	0.23	bdl	bdl	bdl	bdl	0.13	0.41	0.56	0.52	0.29	0.16	0.31
K_2O	0.54	0.12	bdl	bdl	bdl	0.12	bdl	0.11	bdl	bdl	bdl	bdl	bdl	0.03	0.02	bdl	bdl	0.12	bdl	bdl
P_2O_5	bdl	bdl	bdl	bdl	bdl	bdl	bdl	0.18	0.25	0.27	0.24	0.17	0.10	0.18	bdl	bdl	0.06	bdl	bdl	0.23
V_2O_3	bdl	0.45	bdl	bdl	bdl	0.45	bdl	bdl	bdl	0.06	0.02	0.05	0.03	0.07	0.08	bdl	bdl	0.06	bdl	0.39
BaO	bdl	0.15	0.26	bdl	0.26	0.15	bdl	0.20	bdl	bdl	bdl	bdl	bdl	0.07	0.15	0.26	0.16	0.25	0.49	bdl
Cl^-	0.18	0.12	0.52	0.18	0.52	0.12	0.81	bdl	bdl	0.23	0.20	0.17	0.26	0.14	0.22	0.52	0.32	1.12	bdl	bdl
SO_3	1.18	0.18	0.91	0.43	0.91	0.18	0.67	bdl	0.22	bdl	bdl	bdl	0.07	0.09	0.16	0.21	1.70	1.14	0.13	0.27
Total	100.00	100.00	100.00	100.00	100.00	100.00	100.00	100.00	100.00	100.00	100.00	100.00	100.00	100.00	100.00	100.00	100.00	100.00	100.00	100.00
$SiO_2 + Al_2O_3 + Fe_2O_3$	2.61	3.49	3.45	4.86	3.45	4.49	2.61	1.90	2.55	2.15	4.28	4.17	3.34	3.95	4.97	2.50	2.67	4.56	3.85	3.65
$CaO + MgO$	94.51	94.91	94.31	93.88	94.31	93.91	94.51	97.06	95.79	96.64	94.71	95.13	95.64	95.12	93.99	95.96	94.51	92.41	95.38	95.05
HI	0.03	0.04	0.04	0.05	0.04	0.05	0.03	0.02	0.03	0.02	0.05	0.04	0.03	0.04	0.05	0.03	0.03	0.05	0.04	0.04

Table 5. Major element concentrations of binder (B) in *Villa del Pezzolo* mortars (in wt.%; recalculated to 100%; bdl: below detection limits). $SiO_2 + Al_2O_3 + Fe_2O_3$, $CaO + MgO$, HI (Hydraulic Index) are also shown.

| wt.%	VP1 B	VP2 B	VP3 B	VP4 B	VP5 B	VP6 B	VP7 B	VP8 B	VP9 B	VP10 B	VP11 B	VP12 B	VP13 B	VP14 B	VP15 B	VP16 B	VP17 B	VP18 B	VP19 B	VP20 B
SiO_2	9.56	9.52	7.60	9.60	9.73	10.32	5.84	5.72	3.36	6.79	8.81	10.00	9.74	10.17	9.98	8.59	9.84	7.85	12.70	13.81
TiO_2	0.41	bdl	bdl	bdl	0.25	0.07	0.40	bdl	bdl	bdl	0.40	0.20	0.06	bdl	0.14	bdl	0.27	bdl	0.44	0.42
Al_2O_3	5.65	3.13	3.95	4.61	2.48	2.14	3.16	3.20	5.58	3.77	1.69	1.96	4.16	2.51	3.19	6.01	3.17	4.42	3.82	5.73
Fe_2O_3	bdl	0.33	0.70	0.37	bdl	0.53	0.54	0.23	0.12	0.19	bdl	0.12	0.38	0.20	0.23	0.31	0.58	0.28	1.27	bdl
MnO	bdl	0.11	bdl	bdl	bdl	0.08	bdl	bdl	bdl	bdl	0.48	0.03	0.12	0.14	0.08	bdl	0.09	bdl	bdl	bdl
MgO	7.01	1.51	3.08	2.12	3.18	2.02	1.17	6.57	0.21	1.42	1.74	1.18	1.14	1.12	1.02	11.42	5.22	0.06	7.78	12.86
CaO	75.95	79.38	80.25	79.37	80.95	80.44	86.49	82.70	88.86	84.83	85.58	83.07	83.08	83.23	82.44	71.97	78.71	85.52	71.74	65.64
Na_2O	0.23	0.88	0.56	0.36	0.83	0.28	0.41	0.24	0.23	0.89	0.37	0.53	0.88	0.08	0.28	0.17	0.87	0.03	0.53	0.19
K_2O	bdl	1.25	0.49	0.16	0.74	0.95	0.45	bdl	bdl	0.43	0.24	bdl	0.08	0.06	0.07	bdl	0.13	bdl	0.30	bdl
P_2O_5	bdl	0.14	0.00	0.11	0.08	0.11	bdl	bdl	bdl	bdl	0.30	0.08	0.14	0.09	0.11	bdl	0.09	bdl	bdl	bdl
V_2O_3	bdl	bdl	0.44	bdl	0.13	0.24	bdl	0.23	0.29	bdl	bdl	0.15	bdl	bdl	0.14	0.07	bdl	bdl	bdl	bdl
BaO	bdl	bdl	0.53	0.04	0.05	0.10	bdl	bdl	bdl	1.01	0.14	0.05	bdl	0.03	0.10	0.33	bdl	bdl	bdl	bdl
Cl^-	0.37	0.22	0.46	0.36	0.47	0.19	1.41	0.78	0.05	0.10	0.26	0.57	0.16	0.26	0.19	0.23	0.52	0.45	0.83	0.31
SO_3	0.82	3.52	1.96	2.90	1.11	2.53	0.12	0.34	0.30	0.56	bdl	2.05	0.05	2.10	2.03	0.89	0.78	1.12	0.60	1.04
Total	100.00	100.00	100.00	100.00	100.00	100.00	100.00	100.00	99.00	100.00	100.00	100.00	100.00	100.00	100.00	100.00	100.00	100.00	100.00	100.00
$SiO_2 + Al_2O_3 + Fe_2O_3$	15.21	12.98	12.24	14.58	12.21	12.99	9.54	9.15	9.06	10.76	10.49	12.08	14.28	12.88	13.40	14.92	13.59	12.55	17.79	19.54
$CaO + MgO$	82.96	80.89	83.33	81.49	84.13	82.46	87.66	89.27	89.08	86.25	87.32	84.25	84.22	84.35	83.46	83.39	83.93	85.58	79.52	78.50
HI	0.18	0.16	0.15	0.18	0.15	0.16	0.11	0.10	0.10	0.12	0.12	0.14	0.17	0.15	0.16	0.18	0.16	0.15	0.22	0.25
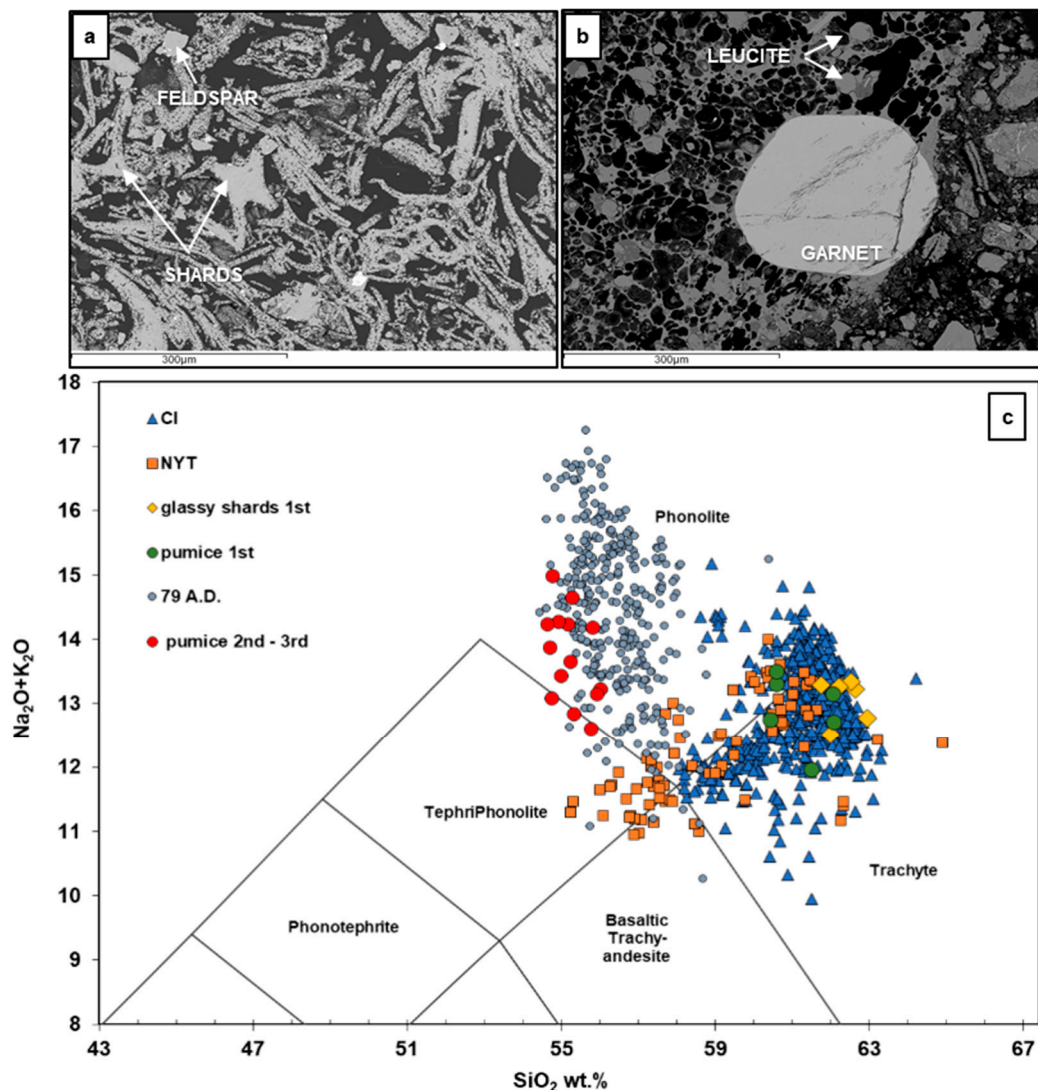
Figure 8. (**a**) Backscattered SEM image of glassy shards partially coated by a thin layer of micrometric sanidine in VP2 sample; (**b**) backscattered SEM image of leucite bearing pumice with garnet in VP14 sample; (**c**) classification of glassy shards and pumice fragments in *Villa del Pezzolo* mortars compared with *Campi Flegrei* and 79 A.D. Somma-Vesuvius volcanic glasses (CI; NYT; 79 A.D.; [38], using a TAS diagram [36]). Abbreviations: CI: Campanian Ignimbrite; NYT: Neapolitan Yellow Tuff; 79 A.D: 79 A.D. Somma-Vesuvius eruption; VP: *Villa del Pezzolo* pumice.

4.4. Thermogravimetric Analysis

Thermal analyses evidenced, for all samples, presence of: (1) carbon-dioxide content, derived from the dissociation of carbonatic phases and (2) structural bound water (SBW), which represents the amount of OH groups occurring in the silicate framework and inside the thinnest ultramicropores [29].

The highest SBW content was reported for sample VP17 (10.6%), while the lowest SBW was reported in samples VP19 and VP20 (3.94–3.45% respectively), also showing the lowest total LOI (Loss On Ignition; 23.76–24.09%); the latter samples were, in fact, floor mortars different from other bedding mortars.

CO_2 values ranged from 4.33% (sample VP13) to 8.02% (sample VP17), except once again for samples V19 and VP20, which highlighted very high CO_2 values (15.82–16.99%, respectively).

According to the Moropoulou et al. [31] diagram (Figure 9) and the CO_2/SBW ratio (lower than 3%; Table 6), all mortars could be defined as natural pozzolanic mortar (Figure 9).
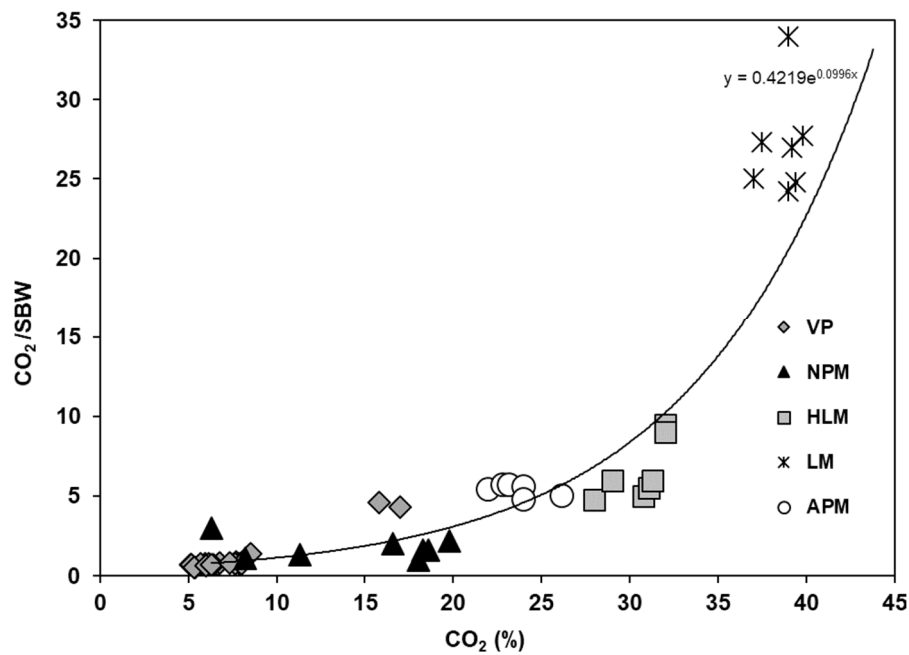
Figure 9. Binary CO_2/SBW vs. CO_2 (%) diagram utilized to compare the obtained data from *Villa del Pezzolo* mortars (VP samples; dark grey diamonds) and those of Moropoulou et al. [31]; (NPM: natural pozzolanic mortars; APM: artificial pozzolanic mortars; HLM: hydraulic lime mortars; LM: lime mortars).

Table 6. Thermal analysis features of investigated samples. Abbreviations: SBW: Structural Boundary Water; LOI: Loss on Ignition.

Sample	SBW%	CO_2%	CO_2/SBW	LOI
VP1	8.72	7.69	0.89	25.23
T range (°C)	200–675	675–780		25–1000
VP2	8.07	5.93	0.73	26.39
T range (°C)	200–670	670–760		25–1000
VP3	10.38	5.40	0.52	28.39
T range (°C)	200–660	660–740		25–1000
VP4	9.14	6.69	0.73	29.06
T range (°C)	230–640	660–750		25–1000
VP5	10.32	7.89	0.77	26.35
T range (°C)	235–610	650–750		25–1000
VP6	8.12	6.17	0.76	27.45
T range (°C)	200–570	640–760		25–1000
VP7	6.07	8.52	1.40	26.31
T range (°C)	180–560	560–780		25–1000
VP8	7.49	5.13	0.69	27.25
T range (°C)	200–640	640–745		25–1000
VP9	7.33	5.15	0.70	28.10
T range (°C)	180–620	620–760		25–1000
VP10	8.35	6.77	0.81	29.25
T range (°C)	200–570	570–750		25–1000
VP11	7.64	5.69	0.74	32.47
T range (°C)	200–650	650–780		25–1000
VP12	10.05	7.63	0.76	35.22
T range (°C)	210–630	630–780		25–1000
VP13	9.77	4.33	0.55	30.21
T range (°C)	180–630	630–740		25–1000

Table 6. *Cont*.

Sample	SBW%	CO$_2$%	CO$_2$/SBW	LOI
VP14	8.98	6.02	0.67	26.76
T range (°C)	220–600	600–740		25–1000
VP15	9.15	6.42	0.70	29.90
T range (°C)	220–640	640–760		25–1000
VP16	9.35	6.31	0.67	25.50
T range (°C)	240–630	630–750		25–1000
VP17	10.67	8.02	0.76	29.36
T range (°C)	240–650	650–740		25–1000
VP18	8.80	7.35	0.84	25.69
T range (°C)	230–620	620–750		25–1000
VP19	3.94	16.99	4.31	24.09
T range (°C)	240–650	650–740		25–1000
VP20	3.45	15.82	4.59	23.78
T range (°C)	160–540	540–780		25–1000

4.5. Mercury Intrusion Porosimetry

The porosity was determined on fragments of selected mortars (VP1, VP8, VP11, VP20) due to the scarcity of available material. Table 7 summarizes the parameters, such as cumulative volume, bulk density, apparent density, open porosity and specific surface, provided by MIP. For each sample, the representative pore size distribution is also shown (Figure 10).

Table 7. Porosimetric features of *Villa del Pezzolo* mortars.

Sample	VP1	VP8	VP15	VP20
Cumulative volume (mm^3/g)	262.11	284.97	307.29	282.37
Bulk density (g/cm^3)	1.64	1.52	1.46	1.50
Apparent Density (g/cm^3)	2.74	2.66	2.65	2.62
Open porosity (vol.%)	40.42	42.96	44.65	42.46
Specific surface (m^2/g)	24.25	31.02	15.68	20.06

As regards the relative volume curves, pore radii mainly range between 5 and 100 nm, except for VP20, where a displacement of the pore access radius towards larger sizes (1000–10,000 nm) was recognized (Figure 10).

The open porosity is very similar for all samples, ranging from 42.46 to 44.65 vol.% (Table 7) with unimodal and broadened shape of the cumulative pore size distribution. Once again, the curve for sample VP20 is more irregular (Figure 10).
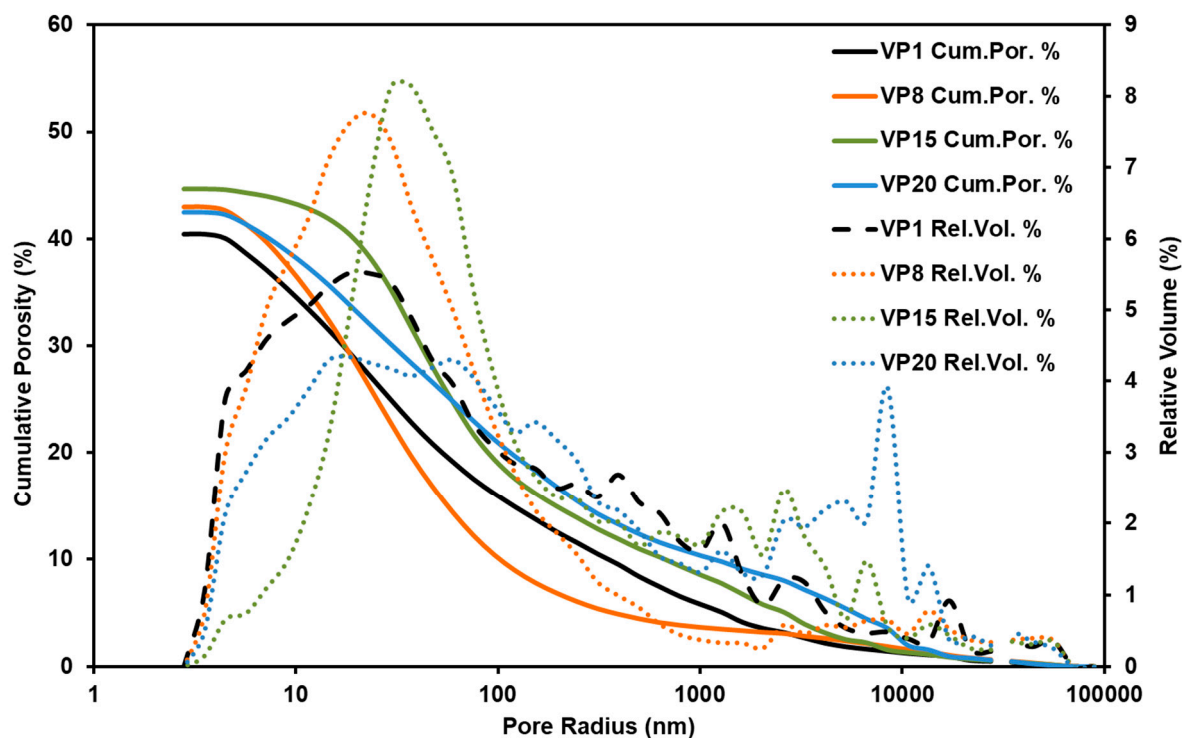
Figure 10. Cumulative (continuous line) and relative (dashed line) pore size distribution of *Villa del Pezzolo* mortars (VP1, VP8, VP15, VP20).

5. Discussion

This research represents a first archaeometric study on mortars from *Villa del Pezzolo* and provides some useful information about mix-design, provenance of raw materials and reconstruction of building phases.

Analytical results allowed for identification of two different mix designs, for bedding and floor mortars, respectively. Bedding mortars were characterized by a mixture of lime, fine volcanic materials, different type of aggregates and water, while floor mortars represent the *cocciopesto*, due to the addition of fictile materials both as binder and aggregates. *Cocciopesto*, also known as *opus signinum*, represents the typical mix design used during the Roman age for waterproof mortars in water tanks, thermal pools, and in the caverns of aqueducts and for flooring [8].

As far as provenance of raw materials is concerned, the minero-petrographic and chemical analyses, along with the surrounding geological setting, confirmed a local origin and also the hypotheses of the three building phases of *Villa del Pezzolo* [18,21].

Volcanic fragments used as aggregate in the first building phase can be related to Campanian Ignimbrite formation, cropping out in the same geographical area (Figure 11). This hypothesis was also confirmed by the presence of specific zeolitic phases (chabazite and analcime; Table 3) and of glassy shards, partially devitrified and replaced by authigenic feldspar (Figure 8a), a typical feature of the welded gray Campanian Ignimbrite lithofacies (CI-WGI; [39]).

Furthermore, chemical composition of glassy shards and pumice fragments follows the compositional trend of CI (Figure 8c).

Regarding the volcanic aggregates used in the mix design of the second and third building phases (after A.D. 79 Somma-Vesuvius eruption), some differences can be evidenced, mostly related to the mineralogical composition and aggregates shape (from angular to sub-rounded). The presence of leucite-bearing scoriae and crystal fragments of garnet, both in binder and pumice, allowed us to relate these materials to eruptive products of Somma-Vesuvius. Chemical composition of garnets (solid solution between andradite 52.99–57.29 mol.% and grossular 25.64–28.65 mol.%) is fully compatible with

Somma-Vesuvius garnets (andradite 46–70 mol.% and grossularia 16–45 mol.%; [41] and unpublished garnets analyzed by Melluso from intrusive Somma-Vesuvius rocks; S3). Moreover, the chemical analysis of pumice, reported in the TAS diagram (Figure 8c) is likely that of Somma-Vesuvius products.
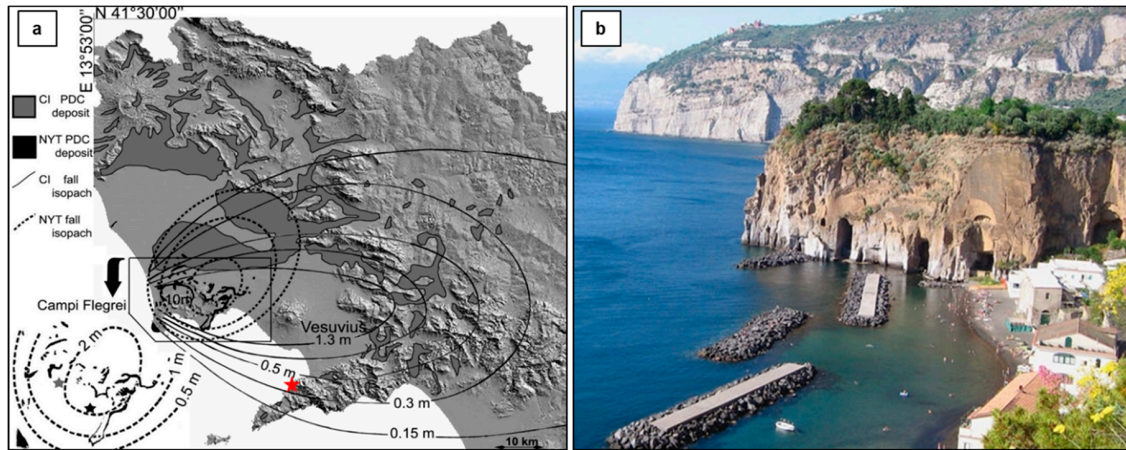

Figure 11. (**a**) distribution of Campanian Ignimbrite (CI) and Neapolitan Yellow Tuff (NYT) pyroclastic density current (PDC) deposits and fall deposits (modified after Scarpati, and Perrotta, [40]). Inset (left) shows their source area (*Campi Flegre*i) and presumed vent locations (black star—NYT vent; gray star—CI vent; red star—*Villa del Pezzolo* location); (**b**) CI-WGI cliff, Piano di Sorrento.

Furthermore, the presence of sub-rounded shaped aggregates allowed us to also hypothesize the use of "Durece" formation, an alluvial delta lithofacies formed by the products of debris- and mud-flows emplaced after strong rainfalls following the Somma-Vesuvius eruption [5].

The samples from the third building phase showed the presence of fictile fragments that are absent in the other building phases. POM observations evidenced that the fictile fragments are very different from each other in terms of matrix, textural and petrographic features. For these reasons, their provenance was hard to define; however, these differences suggest a recycling of building materials. These fictile fragments also have a technological role because they were used to provide hydraulicity to mortars [8,42], as also confirmed by the HI evaluation.

There is no specific information about the provenance of lime and carbonatic aggregates can be provided, but it is reasonable to suggest a local provenance due to the geographical position of the villa, very close to the northern flank of the Lattari Mounts (Mesozoic limestones; Figure 2a).

Composition of the cementiceous binding matrix, in some samples, showed the ubiquitous presence of lime lumps, gypsum and C–A–S–H gel, the latter derived from lime and pozzolanic material reactions (volcanic and fictile materials, [43]); its formation testifies to the achievement of mortar hydraulicity [23,44]

Lime lumps are likely connected to not-well-reacted lime, the origin of which has to be searched in the properties of slaked lime (calcium hydroxide) and in the water/quicklime ratio [10,45]. Chemical analysis of lime lumps (CaO more than 92%) testified to the good nature of limestone used for lime production.

Gypsum can be ascribed to late sulphation of calcite or even reaction between sulfate and hydrated lime [46,47]. Halite in all samples can be easily related to interaction with seawater due to site location.

A common feature of the investigated mortars is the hydraulicity features, confirmed by SEM-EDS and thermal analyses. The evaluated HI index allowed us to consider all mortars as hydraulic exclusively thanks to the addition of materials with pozzolanic activity (volcanic and fictile materials). The role of pozzolanic materials was evident by the HI values evaluated on lime lumps (<0.10%) and binder (0.10–0.25%) that can be classified as quicklime and weakly-moderately hydraulic materials [30,48].

Differences among HI index values (Tables 4 and 5; Figure 7c) further confirmed three building phases, evidencing a low value of HI (0.11–0.14%) for mortars of group A, average values (0.15–018%)

for mortars of group B, and high values (0.15–0.25%) for group C. The higher HI index of group C is due to use of fictile fragments that improve the hydraulicity of mortars.

Hydraulicity of mortars was also further established by the results of thermal analyses, which showed weight loss of Structural Bound Water (SBW, 200–600 °C), generally related to the presence of hydrated compounds such as C–A–S–H, and the decomposition of calcite and other carbonates, usually occurring between 600–850 °C with a consequent release of CO_2 (Table 6; [29,49]). According to the literature data [31,50], the binary diagram CO_2/SBW vs. CO_2 (Figure 9) classified all analyzed mortars as natural pozzolanic.

The high concentration of secondary mineralogical phases, the C–A–S–H gel, was supported by porosity tests, which showed a maximum in pore radius distribution between 5 and 100 nm and an open porosity between 40–45 vol.% (Figure 10; Table 7). Small dimension of pore radius is due to the formation of C–A–S–H gel that fills the pores enhancing bonding in pumice clasts and improving resistance to weathering [9,34,51]. According to Sutter [52], the pore radius range is important for material durability: the range between 5 and 100 nm is considered not detrimental for durability, while the range 1000–10,000 nm, detected for sample VP20, can promote weathering [53,54].

The analyses of the mortars used in the construction of *Villa del Pezzolo* revealed important evidence with regard to reconstruction of building phases according to the hypothesis performed by archaeologists and geologists [5,19,21].

Generally, this analytical approach can provide important information about techniques used in the preparation of ancient mortars, and thus they can be used as references for future comparative studies, also involving other buildings in coeval constructions.

This research demonstrates that studying minor sites such as *Villa del Pezzolo* is very important and useful as, similarly to Pompeii, they experienced the effects of the A.D. 79 Somma-Vesuvius eruption and of debris and mud flows generated after this event. It is also very important to focus the attention to this kind of archaeological sites in order to improve the conservation state and fruition by the public.

References

1. De Bonis, A.; Febbraro, S.; Germinario, C.; Giampaola, D.; Grifa, C.; Guarino, V.; Langella, A.; Morra, V. Distinctive Volcanic Material for the Production of Campana a Ware: The Workshop Area of Neapolis at the Duomo Metro Station in Naples, Italy. *Geoarchaeology* **2016**, *31*, 437–466. [CrossRef]
2. Guarino, V.; De Bonis, A.; Faga, I.; Giampaola, D.; Grifa, C.; Langella, A.; Liuzza, V.; Pierobon Benoit, R.; Romano, P.; Morra, V. Production and circulation of thin walled pottery from the Roman port of Neapolis, Campania (Italy). *Period. Mineral.* **2016**, *85*, 95–114.

3.   Di Benedetto, C.; Graziano, S.F.; Guarino, V.; Rispoli, C.; Munzi, P.; Morra, V.; Cappelletti, P. Romans' established skills: Mortars from D46b Mausoleum, Porta Mediana Necropolis, Cuma (Naples). *Mediterr. Archaeol. Archaeom.* **2018**, *18*, 131–146.

4.   Graziano, S.F.; Di Benedetto, C.; Guarino, V.; Rispoli, C.; Munzi, P.; Cappelletti, P.; Morra, V. Technology and building materials in Roman age (1st BC—2nd AD): The "Mausoleo Della Sfinge" from the archaeological site of Cuma (Italy). *Mediterr. Archaeol. Archaeom.* **2018**, *18*, 81–94.

5.   Aucelli, P.; Cinque, A.; Mattei, G.; Pappone, G. Historical sea level changes and effects on the coasts of Sorrento Peninsula (Gulf of Naples): New constrains from recent geoarchaeological investigations. *Palaeogeogr. Palaeoclimatol. Palaeoecol.* **2016**, *463*, 112–125. [CrossRef]

6.   Moropoulou, A.; Bakolas, A.; Bisbikou, K. Investigation of the technology of historic mortars. *J. Cult. Herit.* **2000**, *1*, 45–58. [CrossRef]

7.   Moropoulou, A.; Cakmak, A.; Labropoulos, K.C.; Van Grieken, R.; Torfs, K. Accelerated microstructural evolution of a calcium-silicate-hydrate (C-S-H) phase in pozzolanic pastes using fine siliceous sources: Comparison with historic pozzolanic mortars. *Cem. Concr. Res.* **2004**, *34*, 1–6. [CrossRef]

8.   Collepardi, M. La lezione dei romani: Durabilità e sostenibilità delle opere architettoniche e strutturali. In Proceedings of the III Convegno AIMAT "Restauro e Conservazione dei Beni Culturali: Materiali e Tecniche", Cassino, Italy, 3–4 October 2003.

9.   Jackson, M.D.; Mulcahy, S.R.; Chen, H.; Li, Y.; Li, Q.; Cappelletti, P.; Wenk, H.R. Phillipsite and Al-tobermorite mineral cements produced through low-temperature water-rock reactions in Roman marine concrete. *Am. Mineral.* **2017**, *102*, 1435–1450. [CrossRef]

10.   Jackson, M.D.; Oleson, J.P.; Moon, J.; Zhang, Y.; Chen, H.; Gudmundsson, M.T. Extreme durability in ancient Roman concretes. *Am. Ceram. Soc. Bull.* **2018**, *97*, 22–28.

11.   La Russa, M.F.; Ruffolo, S.A.; Ricca, M.; Rovella, N.; Comite, V.; De Buergo, M.A.; Crisci, G.M.; Barca, D. Archaeometric approach for the study of mortars from the underwater archaeological site of Baia (Naples) Italy: Preliminary results. *Period. Mineral.* **2015**, *84*, 553–567.

12.   Vola, G.; Stanislao, C.; Rispoli, C.; Morra, V.; De Gennaro, M. Petrographic quantitative analysis of pozzolanic mortars from ancient Roman marine concrete cores, drilled by Romacons team (2006–2009). *Rend. Online Soc. Geol. Ital.* **2010**, *11*, 561–562.

13.   Rispoli, C.; Graziano, S.F.; De Bonis, A.; Cappelletti, P.; Esposito, R.; Talamo, P. Piscina Mirabilis: Characterization of geomaterials. In Proceedings of the 1st International Conference on Metrology for Archaeology, Benevento, Italy, 22–23 October 2015; pp. 266–270.

14.   Rispoli, C.; Fedele, L.; Di Benedetto, C.; Esposito, R.; Graziano, S.F.; Guarino, V.; Morra, V.; Cappelletti, P. Characterization of building materials from the Anfiteatro Flavio (Pozzuoli, southern Italy): A mineralogical and petrographic study. *Ital. J. Geosci.* **2019**, *138*, 103–115. [CrossRef]

15.   Izzo, F.; Arizzi, A.; Cappelletti, P.; Cultrone, G.; De Bonis, A.; Germinario, C.; Graziano, S.F.; Grifa, C.; Guarino, V.; Mercurio, M. The art of building in the Roman period (89 B.C.—79 A.D.): Mortars, plasters and mosaic floors from ancient Stabiae (Naples, Italy). *Constr. Build. Mater.* **2016**, *117*, 129–143. [CrossRef]

16.   Rispoli, C. Ancient Roman Mortars: Mix Design, Mineralogical Composition and Minerogenetic Secondary Processes. Ph.D. Thesis, Federico II University of Naples, Naples, Italy, 2017.

17.   Vitale, S.; Tramparulo, F.D.; Ciarcia, S.; Amore, F.O.; Prinzi, E.P.; Laiena, F. The northward tectonic transport in the southern Apennines: Examples from the Capri Island and western Sorrento Peninsula (Italy). *Int. J. Earth Sci.* **2017**, *106*, 97–113. [CrossRef]

18.   Cinque, A.; Robustelli, G.; Russo, M. The consequences of pyroclastic fallout on the dynamics of Mountain Catchments: Geomorphic events in the Rivo D'Arco Basin Sorrento Peninsula Italy after the plinian eruption of vesuvius in 79 Ad. *Geogr. Fis. Din. Quat.* **2000**, *23*, 117–129.

19.   Cinque, A.; Robustelli, G. Alluvial and coastal hazards caused by long-range effects of Plinian eruptions: The case of the Lattari Mts. After the AD 79 eruption of Vesuvius. *Geol. Soc. Spec. Publ.* **2009**, *322*, 155–171. [CrossRef]

20.   Senatore, M.R.; Ciarallo, A.; Stanley, J.-D. Pompeii damaged by volcaniclastic debris flows triggered centuries prior to the 79 A.D. vesuvius eruption. *Geoarchaeology* **2014**, *29*, 1–15. [CrossRef]

21.   Mingazzini, P. *Forma Italiae: Latium et Campania. Surrentum*; Roma De Luca: Roma, Italy, 1946.

22.   Adam, J.P. *L'arte di costruire presso i Romani. Materiali e tecniche*; Longanesi: Milano, Italy, 1988.

23. Rispoli, C.; Graziano, S.F.; Guarino, V.; De Bonis, A.; Di Benedetto, C.; Esposito, R.; Budetta, T.; Morra, V.; Cappelletti, P. Characterization of ancient mortars: Preliminary results from Villa del Pezzolo, Sorrento Peninsula, Italy. In Proceedings of the IMEKO International Conference on Metrology for Archeology and Cultural Heritage, MetroArcheo 2016, Torino, Italy, 19–21 October 2016; pp. 151–156.

24. UNI Ente Italiano Di Normazione. *UNI-EN 11305:2009. Beni Culturali: Malte Storiche, Linee Guida per la Caratterizzazione Mineralogico Petrografica, Fisica e Chimica Delle Malte*; UNI: Roma, Italy, 2009.

25. Munsell, A.H. *Color Soil Charts*; Fonte/Imprenta: New Windsor, NY, USA, 1994.

26. Howarth, R.J. Improved estimators of uncertainty in proportions, point-counting, and pass-fail test results. *Am. J. Sci.* **1998**, *298*, 594–607. [CrossRef]

27. Klug, H.P.; Aexander, L.E. *X-ray Diffraction Procedures or Polycrystalline and Amorphous Materials*; J. Wiley and Sons: New York, NY, USA, 1974.

28. Bish, D.; Chipera, S.J. Problems and solution in quantitative analysis of complex mixture by X-ray powder diffraction. *Adv. Xray Anal.* **1988**, *31*, 295–307.

29. Rispoli, C.; De Bonis, A.; Guarino, V.; Graziano, S.F.; Di Benedetto, C.; Esposito, R.; Morra, V.; Cappelletti, P. The ancient pozzolanic mortars of the Thermal complex of Baia (Campi Flegrei, Italy). *J. Cult. Herit.* **2019**. [CrossRef]

30. Boynton, R.S. *Chemistry and Technology of Lime and Limestone*, 2nd ed.; John Wiley & Sons: New York, NY, USA, 1980.

31. Moropoulou, A.; Bakolas, A.; Anagnostopoulou, S. Composite materials in ancient structures. *Cem. Concr. Compos.* **2005**, *27*, 295–300. [CrossRef]

32. Whitney, D.L.; Evans, B.W. Abbreviations for names of rock-forming minerals. *Am. Mineral.* **2010**, *95*, 185–187. [CrossRef]

33. Jackson, M.; Deocampo, D.; Marra, F.; Scheetz, B. Mid-Pleistocene pozzolanic volcanic ash in ancient Roman concretes. *Geoarchaeology* **2010**, *25*, 36–74. [CrossRef]

34. Jackson, M.D.; Chae, S.R.; Mulcahy, S.R.; Meral, C.; Taylor, R.; Li, P.; Emwas, A.-H.; Moon, J.; Yoon, S.; Vola, G.; et al. Unlocking the secrets of Al-tobermorite in Roman seawater concrete. *Am. Mineral.* **2012**, *98*, 1669–1687. [CrossRef]

35. Fernández, R.; Nebreda, B.; De La Villa, R.V.; García, R.; Frías, M. Mineralogical and chemical evolution of hydrated phases in the pozzolanic reaction of calcined paper sludge. *Cem. Concr. Compos.* **2010**, *32*, 775–782. [CrossRef]

36. Le Bas, M.J.; Le Maitre, R.W.; Streckeisen, A.; Zanettin, B. A chemical classification of volcanic rocks based on the total alkali-silica diagram. *J. Petrol.* **1986**, *27*, 745–750. [CrossRef]

37. Locock, A.J. An Excel spreadsheet to recast analyses of garnet into end-member components, and a synopsis of the crystal chemistry of natural silicate garnets. *Comput. Geosci.* **2008**, *34*, 1769–1780. [CrossRef]

38. Morra, V.; Calcaterra, D.; Cappelletti, P.; Colella, A.; Fedele, L.; de Gennaro, R.; Langella, A.; Mercurio, M.; de Gennaro, M. Urban geology: Relationships between geological setting and architectural heritage of the Neapolitan area. *J. Virtual Explor.* **2010**, *36*. [CrossRef]

39. Langella, A.; Bish, D.L.; Cappelletti, P.; Cerri, G.; Colella, A.; de Gennaro, R.; Graziano, S.F.; Perrotta, A.; Scarpati, C.; de Gennaro, M. New insights into the mineralogical facies distribution of Campanian Ignimbrite, a relevant Italian industrial material. *Appl. Clay Sci.* **2013**, *72*, 55–73. [CrossRef]

40. Scarpati, C.; Perrotta, A. Erosional characteristics and behavior of large pyroclastic density currents. *Geology* **2012**, *40*, 1035–1038. [CrossRef]

41. Scheibner, B.; Wörner, G.; Civetta, L.; Stosch, H.-G.; Simon, K.; Kronz, A. Rare earth element fractionation in magmatic Ca-rich garnets. *Contrib. Mineral. Petrol.* **2007**, *154*, 55–74. [CrossRef]

42. Baronio, G.; Binda, L. Study of the pozzolanicity of some bricks and clays. *Constr. Build. Mater.* **1997**, *11*, 41–46. [CrossRef]

43. De Luca, R.; Miriello, D.; Pecci, A.; Dominguez-Bella, S.; Bernal-Casasola, D.; Cottica, D.; Bloise, A.; Crisci, G.M. Archaeometric Study of Mortars from the Garum Shop at Pompeii, Campania, Italy. *Geoarchaeology* **2015**, *30*, 330–351. [CrossRef]

44. Middendorf, B.; Knöfel, D. Gypsum and lime mortars of historic German brick buildings: Analytical results as well as requirements for adapted restoration material. In *Conservation of Historic Brick Structures: Case Studies and Reports of Research*; Baer, N.S., Fitz, S., Livingston, R.A., Eds.; Donhead publishing: Shaftsbury, UK, 1998.

45. Barba, L.; Blancas, J.; Manzanilla, L.R.; Ortiz, A.; Barca, D.; Crisci, G.M.; Miriello, D.; Pecci, A. Provenance of the limestone used in Teotihuacan (Mexico): A methodological approach. *Archaeometry* **2009**, *51*, 525–545. [CrossRef]

46. De Gennaro, M.; Colella, C.; Pansini, M. Hydrothermal conversion of trachytic glass into zeolite. II Reactions with high-salinity waters. *Neues Jahrb. Far Mineral.* **1993**, *3*, 97–110.

47. Stanislao, C.; Rispoli, C.; Vola, G.; Cappelletti, P.; Morra, V.; De Gennaro, M. Contribution to the knowledge of ancient Roman seawater concretes: Phlegrean pozzolan adopted in the construction of the harbour at Soli-Pompeiopolis (Mersin, Turkey). *Period. Mineral.* **2011**, *80*, 471–488.

48. Zawawi, R. Artificial hydraulic lime mortar obtained by calcining limestone and siliceous waste materials. *J. Adv. Appl. Ceram.* **2006**, *10*, 175–178. [CrossRef]

49. Izzo, F.; Grifa, C.; Germinario, C.; Mercurio, M.; De Bonis, A.; Tomay, L.; Langella, A. Production technology of mortar-based building materials from the Arch of Trajan and the Roman Theatre in Benevento, Italy. *Eur. Phys. J. Plus* **2018**, *133*, 1–12. [CrossRef]

50. Genestar, C.; Pons, C.; Más, A. Analytical characterisation of ancient mortars from the archaeological Roman city of Pollentia (Balearic Islands, Spain). *Anal. Chim. Acta* **2006**, *557*, 373–379. [CrossRef]

51. Brandon, C.J.; Hohlfelder, R.L.; Jackson, M.D.; Oleson, J.P. *Building for Eternity. The History and Technology of Roman Concrete Engineering in the Sea*; Oxbow Books: Oxford, UK, 2014.

52. Sutter, L. *Mineral Characterization and Cataloging of Quarried Aggregate Sources. Volume I: Final Report*; Michigan Department of Transportation: Lansing, MI, USA, 2005.

53. Cultrone, G.; Sebastián, E.; Huertas, M.O. Durability of masonry systems: A laboratory study. *Constr. Build. Mater.* **2007**, *21*, 40–51. [CrossRef]

54. Ontiveros-Ortega, E.; Rodríguez-Gutiérrez, O.; Navarro, A.D. Mineralogical and physical-chemical characterisation of Roman mortars used for monumental substructures on the hill of San Antonio, in the Roman city of Italica (prov. Baetica, Santiponce, Seville, Spain). *J. Archaeol. Sci. Rep.* **2016**, *7*, 205–223. [CrossRef]